

# Developed turbulence and nonlinear amplification of magnetic fields in laboratory and astrophysical plasmas

Jena Meinecke<sup>a,1</sup>, Petros Tzeferacos<sup>b</sup>, Anthony Bell<sup>a</sup>, Robert Bingham<sup>c,d</sup>, Robert Clarke<sup>c</sup>, Eugene Churazov<sup>e,f</sup>, Robert Crowston<sup>g</sup>, Hugo Doyle<sup>a</sup>, R. Paul Drake<sup>h</sup>, Robert Heathcote<sup>c</sup>, Michel Koenig<sup>i</sup>, Yasuhiro Kuramitsu<sup>j,k</sup>, Carolyn Kuranz<sup>h</sup>, Dongwook Lee<sup>l</sup>, Michael MacDonald<sup>h</sup>, Christopher Murphy<sup>g</sup>, Margaret Notley<sup>c</sup>, Hye-Sook Park<sup>m</sup>, Alexander Pelka<sup>i,n</sup>, Alessandra Ravasio<sup>i</sup>, Brian Reville<sup>o</sup>, Youichi Sakawa<sup>k</sup>, Willow Wan<sup>h</sup>, Nigel Woolsey<sup>g</sup>, Roman Yurchak<sup>i</sup>, Francesco Miniati<sup>p</sup>, Alexander Schekochihin<sup>a</sup>, Don Lamb<sup>b</sup>, and Gianluca Gregori<sup>a,b,1</sup>

<sup>a</sup>Department of Physics, University of Oxford, Oxford OX1 3PU, United Kingdom; <sup>b</sup>Department of Astronomy and Astrophysics, University of Chicago, Chicago, IL 60637; <sup>c</sup>Rutherford Appleton Laboratory, Didcot OX11 0QX, United Kingdom; <sup>d</sup>Department of Physics, University of Strathclyde, Glasgow G4 0NG, United Kingdom; <sup>e</sup>Max Planck Institute for Astrophysics, D-85741 Garching, Germany; <sup>f</sup>Space Research Institute, Moscow 117997, Russia; <sup>g</sup>Department of Physics, University of York, York YO10 5D, United Kingdom; <sup>h</sup>Atmospheric, Oceanic and Space Sciences, University of Michigan, Ann Arbor, MI 48109; <sup>i</sup>Laboratoire pour l'Utilisation de Lasers Intenses, UMR7605, CNRS Commissariat à l'Énergie Atomique et aux Énergies Alternatives, Université Paris VI Ecole Polytechnique, F-91128 Palaiseau Cedex, France; <sup>j</sup>Department of Physics, National Central University, Taoyuan 320, Taiwan; <sup>k</sup>Institute of Laser Engineering, Osaka University, Osaka 565-0871, Japan; <sup>l</sup>Applied Mathematics and Statistics, University of California, Santa Cruz, CA 96064; <sup>m</sup>Lawrence Livermore National Laboratory, Livermore, CA 94550; <sup>n</sup>Institute of Radiation Physics, Helmholtz-Zentrum Dresden-Rossendorf, D-01314 Dresden, Germany; <sup>o</sup>School of Mathematics and Physics, Queens University Belfast, Belfast BT7 1NN, United Kingdom; and <sup>p</sup>Department of Physics, ETH Zürich, CH-8093 Zürich, Switzerland

Edited by Neta A. Bahcall, Princeton University, Princeton, NJ, and approved May 19, 2015 (received for review February 1, 2015)

**The visible matter in the universe is turbulent and magnetized. Turbulence in galaxy clusters is produced by mergers and by jets of the central galaxies and believed responsible for the amplification of magnetic fields. We report on experiments looking at the collision of two laser-produced plasma clouds, mimicking, in the laboratory, a cluster merger event. By measuring the spectrum of the density fluctuations, we infer developed, Kolmogorov-like turbulence. From spectral line broadening, we estimate a level of turbulence consistent with turbulent heating balancing radiative cooling, as it likely does in galaxy clusters. We show that the magnetic field is amplified by turbulent motions, reaching a nonlinear regime that is a precursor to turbulent dynamo. Thus, our experiment provides a promising platform for understanding the structure of turbulence and the amplification of magnetic fields in the universe.**

galaxy clusters | laboratory analogues | lasers | magnetic fields | turbulence

In the early universe, matter was nearly homogeneously distributed; today, as a result of gravitational instabilities, it forms a web-like structure consisting of filaments and galaxy clusters (1). The continued mergers of galaxies, filaments, and galaxy clusters inject turbulence into the intergalactic medium via shocks (2, 3). At the same time, the existence of diffuse synchrotron emission at radio wavelengths and Faraday rotation measurements indicate the presence of magnetic fields in galaxy clusters with strengths up to tens of microgausses (4, 5). The standard model for the origin of these intergalactic magnetic fields is amplification of seed fields via the turbulent dynamo mechanism to the present-day observed values (6–10), but other possibilities involving plasma kinetic instabilities (11–14), return currents (15, 16), or primordial mechanisms (17, 18) have also been invoked.

We have carried out experiments involving the collision of two plasma jets—reminiscent of cluster merger events—to produce a laboratory-scale replica of a turbulent intracluster plasma, although obviously our plasma is not confined in a dark matter potential well, as it is in clusters. In the intracluster medium, large-scale turbulent motions are influenced by density stratification and gravity. However, at smaller spatial scales, the time periods for buoyancy-driven motions are much longer than those of the turbulent motions, so the fluctuations at these scales are universal, and thus similar to the turbulence we can create in our laboratory experiments. The scale invariance of hydrodynamic equations (19, 20) implies, if we assume that a distance of 1 cm in

the laboratory corresponds to 100 kiloparsecs in the astrophysical case, that 1  $\mu$ s becomes 0.5 Gy and a density of  $4 \times 10^{17} \text{ cm}^{-3}$  is equivalent to  $0.01 \text{ cm}^{-3}$  in the galaxy cluster.

Our experiments were conducted using the Vulcan laser of the Central Laser Facility at the Rutherford Appleton Laboratory. We have focused multiple laser beams (with  $\sim 240 \text{ J}$  total energy and  $\sim 1$ -ns pulse duration) onto a carbon foil to launch a plasma jet into an ambient argon gas-filled chamber (at a pressure of 1 mbar). A full description of the experimental setup is given in Fig. 1. Ablation of target material by the laser drives a shock into the carbon foil, which then produces a collimated jet from the back surface of the target (i.e., the side opposite to that illuminated by the laser). The target material ablated by the laser is slowed by the ambient medium, creating a wrap-around shock, visible in Fig. 1. Schlieren measurements were

## Significance

**Magnetic fields exist throughout the universe. Their energy density is comparable to the energy density of the fluid motions of the plasma in which they are embedded, making magnetic fields essential players in the dynamics of the luminous matter in the universe. The origin and the amplification of these magnetic fields to their observed strengths are far from being understood. The standard model for the origin of these galactic and intergalactic magnetic fields is through the amplification of seed fields via turbulent processes to the level consistent with current observations. For this process to be effective, the amplification needs to reach a strongly nonlinear phase. Experimental evidence of the initial nonlinear amplification of magnetic fields is presented in this paper.**

Author contributions: B.R., F.M., A.S., D. Lamb, and G.G. conceived the project; J.M., R.B., R.P.D., C.M., B.R., N.W., A.S., and G.G. designed research; J.M., R. Clarke, R. Crowston, H.D., R.H., C.K., M.M., C.M., M.N., A.P., and W.W. carried out Vulcan experiment; J.M., E.C., and H.D. analyzed data; P.T. performed numerical simulations; P.T., A.B., M.K., Y.K., D. Lee, H.-S.P., A.R., B.R., Y.S., N.W., R.Y., F.M., A.S., D. Lamb provided further experimental and theoretical support; and J.M., P.T., A.B., H.D., B.R., A.S., D. Lamb, and G.G. wrote the paper.

The authors declare no conflict of interest.

This article is a PNAS Direct Submission.

<sup>1</sup>To whom correspondence may be addressed. Email: g.gregori1@physics.ox.ac.uk or jena.meinecke@physics.ox.ac.uk.

This article contains supporting information online at [www.pnas.org/lookup/suppl/doi:10.1073/pnas.1502079112/-DCSupplemental](http://www.pnas.org/lookup/suppl/doi:10.1073/pnas.1502079112/-DCSupplemental).

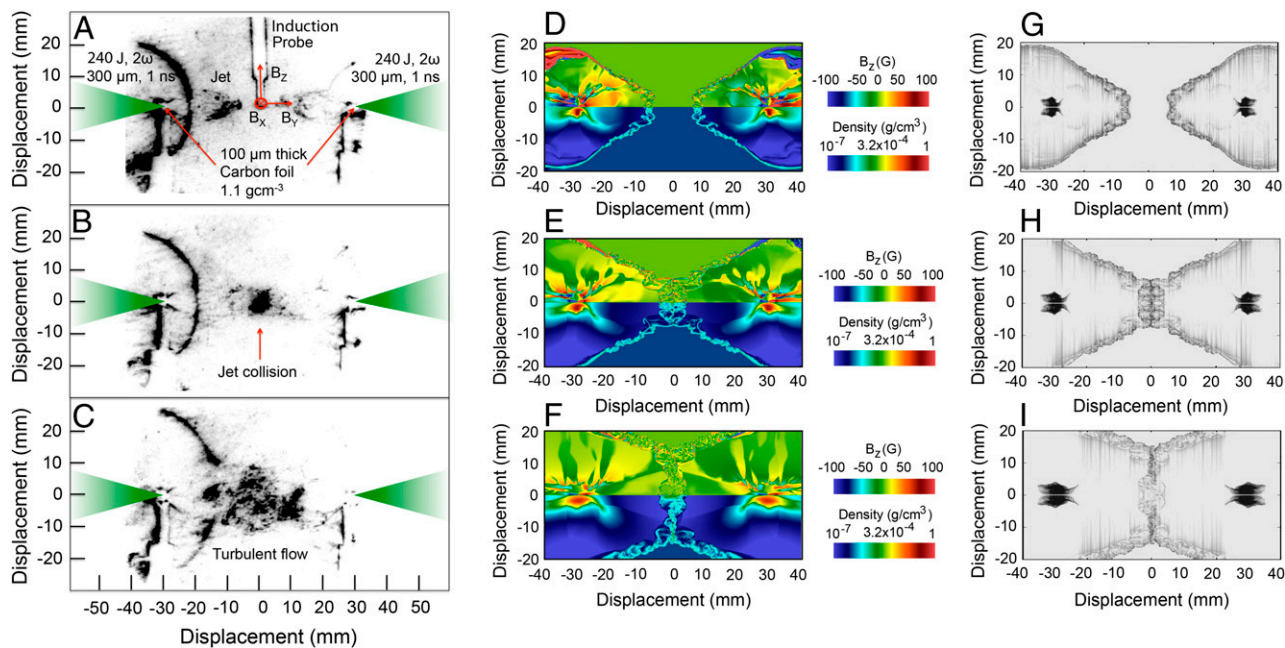


**Fig. 1.** Colliding jet configuration for the generation of turbulence. Two carbon foils ( $100\ \mu\text{m}$  thick, with density  $1.13\ \text{g/cm}^3$ ) are separated by  $60\ \text{mm}$  in a  $1 \pm 0.2\ \text{mbar}$  argon gas-filled chamber. Each target is ablated by three frequency-doubled ( $527\text{-nm}$ -wavelength) laser beams with a laser spot diameter of  $300\ \mu\text{m}$ . The total laser illumination onto each foil is  $240 \pm 30\ \text{J}$  in a  $1\text{-ns}$  pulse length. An induction coil ( $\geq 200\text{-MHz}$  bandwidth, with four twisted pair coils wound around the axis of a  $\sim 1 \times 1\ \text{mm}^2$  plastic core) is placed at equal distance between the foil targets. Additional details are given in ref. 10. (A) Schlieren image (using a  $532\text{-nm}$ -wavelength probe and  $5\text{-ns}$  CCD gate width) of the jet formations at  $t = 500\ \text{ns}$  after the laser shot. (B) The jets collide at  $t = 800\ \text{ns}$ , and (C) turbulence develops by  $t = 1,500\ \text{ns}$ . (D) Magnetic field (Top) and mass density (Bottom) from a FLASH simulation of the two jets at  $t = 500\ \text{ns}$ . (E) Same as D but at  $t = 800\ \text{ns}$ . (F) same as D but at  $t = 1,500\ \text{ns}$ . (g) Schlieren synthetic image obtained by postprocessing the FLASH results at  $t = 500\ \text{ns}$  using Spect3D (34). (H) Same as G but at  $t = 800\ \text{ns}$ . (I) same as G but at  $t = 1,500\ \text{ns}$ . The measured and simulated Schlieren images are similar at  $t = 500\ \text{ns}$  and  $800\ \text{ns}$ , but differ at  $t = 1,500\ \text{ns}$ . The difference is likely due to a slight angle between the directions the two jets are moving, which allows part of the jets to continue beyond the initial interaction region. This produces a much larger turbulent region in the experiment than in the simulation, where the 2D cylindrical geometry prevents us from accommodating this situation. Since the FLASH simulations are 2D cylindrical, the plane that most closely corresponds to the experimental data is the one that is perpendicular to the page and connects the two target foils. This plane does not contain the induction coil probe.

taken to characterize the outflows at various times. The fastest moving material occurs on axis (see Fig. 2) with  $v_0 \approx 25\ \text{km/s}$  ( $v_0/c_s \approx 4$ , where  $c_s$  is the sound speed) at  $3\ \text{cm}$  from the target, while material on the edges of the jet moves more slowly as a result of Kelvin–Helmholtz shearing instabilities. Experiments were also performed using two sets of laser beams, each set illuminating a carbon foil, producing two jets that collide. The collision drives strong turbulence in a region that grows from a size  $L \sim 1\ \text{cm}$  at  $t = 0.8\ \mu\text{s}$  to  $L \approx 2\ \text{cm}$  at  $t > 1.5\ \mu\text{s}$ , at which time the turbulence reaches a more relaxed state.

The turbulent velocity fluctuations on the system scale  $L$  can be estimated from Fig. 2B. At the collision point, the observed argon emission lines are broadened by  $\sim 0.2\ \text{nm}$ . Half of this broadening is attributed to the increased density, and to a lesser extent to the higher temperatures (thermal broadening is small due to the large ion mass) (Supporting Information). The broadening due to turbulent motions is then  $\sim 0.1\ \text{nm}$ , corresponding to a turbulent velocity  $v_{\text{turb}} \approx 27 \pm 5\ \text{km/s}$ . Thus,  $v_{\text{turb}} \approx v_0$ , suggesting that the collision effectively randomizes the directed velocities of the two jets. Taking the measured values of jet velocity, density, and temperature in the collision region, and assuming an ionization state  $Z \approx 2.5$  for argon, we estimate the interjet electron–ion ( $\lambda_{ei} \approx 0.04\ \text{cm}$ ) and ion–ion ( $\lambda_{ii} \approx 0.005\ \text{cm}$ ) mean free paths to be significantly smaller than the size of the jets. This confirms that the two jets strongly interact via Coulomb collisions and the contact surface between the two jets becomes quickly unstable. The Reynolds number calculated with respect to the scale  $L$  is thus  $\text{Re} = v_{\text{turb}}L/\nu \approx 1.0 \times 10^6$  ( $\nu \approx 2.8\ \text{cm}^2/\text{s}$  is the kinematic viscosity of the plasma).

For our plasma conditions, the radiative cooling rate per ion is  $Q_{\text{cool}} \approx m_{\text{ion}}\kappa_P\sigma_{SB}T^4 \approx 0.5\ \text{eV/ns}$ , where  $m_{\text{ion}}$  is the argon mass,  $\kappa_P \approx 8 \times 10^4\ \text{cm}^2/\text{g}$  is the Planck opacity (see Supporting Information), and  $\sigma_{SB}$  is the Stefan–Boltzmann constant. This implies that during one jet crossing time,  $\sim L/v_0 \approx 400\ \text{ns}$ , the plasma should have cooled to near  $1\ \text{eV}$ , as in the case of a single-jet expansion (detailed calculations are provided in Supporting Information). Fig. 2 instead shows that in the collision region the temperature remains  $\geq 2\ \text{eV}$  over a few  $L/v_0$ , suggesting that much of the cooling must be offset by heating. Turbulent motions are eventually dissipated into heat. This heating rate per ion can be approximated to be  $Q_{\text{turb}} \approx m_{\text{ion}}v_{\text{turb}}^3/L \approx 0.6\ \text{eV/ns}$ . Thus,  $Q_{\text{turb}} \approx Q_{\text{cool}}$ , consistent with turbulence playing an important role in achieving a stable temperature profile, with near balance between turbulent heating and radiative cooling.

We performed simulations of the experiments using the FLASH code (21, 22) (see Supporting Information). The results of the FLASH simulations are consistent with the measured properties of the jet, including its morphology and the physical conditions in the interaction region (Figs. 1 and 2). The simulations indicate enhanced vorticity as the two jets collide, and reproduce the increase in the electron density and the moderate rise in the temperature after the collision.

In some respects, our experimental conditions are qualitatively similar to those found in galaxy clusters, where heating driven by turbulent motions in the intracluster plasma reduces radiative losses and decreases the net cooling rate (23). On the other hand, while, in the inertial range, energy is transferred from one scale to another at a rate given by  $Q_{\text{turb}}$ , which has the same form in both clusters and laboratory experiments, the actual

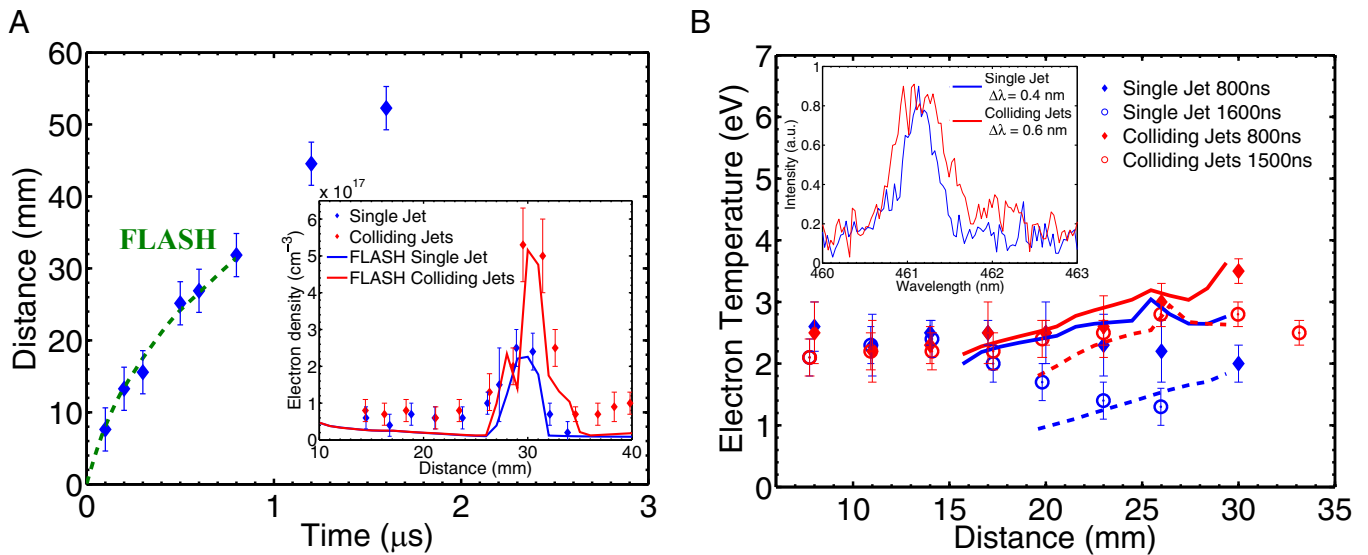


**Fig. 2.** Characterization of jet propagation and collision. (A) Measurement of the jet leading edge vs. time from Schlieren data (blue symbols) and FLASH simulations (dashed green line). The FLASH simulation was calibrated to match the position of the leading edge of the jet at 800 ns for the measured value of the total laser energy for that data point. (Inset) The electron density profile obtained by interferometry at  $t = 800$  ns compared with FLASH predictions. The density has been averaged over a volume of 5 mm radius from the axis connecting the two target foils. (B) Spatially resolved electron temperature profile of a single jet (blue symbols) and colliding jets (red symbols) at  $t = 800$  ns obtained from the measured argon spectral lines (see [Supporting Information](#) for details). Solid lines (blue, single jet; red, colliding jets) correspond to the predicted temperature values from FLASH simulations at  $t = 800$  ns, averaged over the same volume as the electron density. Dashed lines are the results from the same FLASH simulations at  $t = 1,500$  ns. (Inset) An example of the argon spectral line at  $t = 800$  ns and 3 cm from the carbon foil target (averaged over 0.1 cm).

mechanism for energy dissipation into heat can be different. This is dominated by collisional, isotropic viscosity in the laboratory, whereas in clusters, at a minimum, one must take into account

that viscosity is anisotropic due to magnetic fields, and, furthermore, kinetic processes may play an important role (8). Thus, the similarity between the laboratory “replica” and the

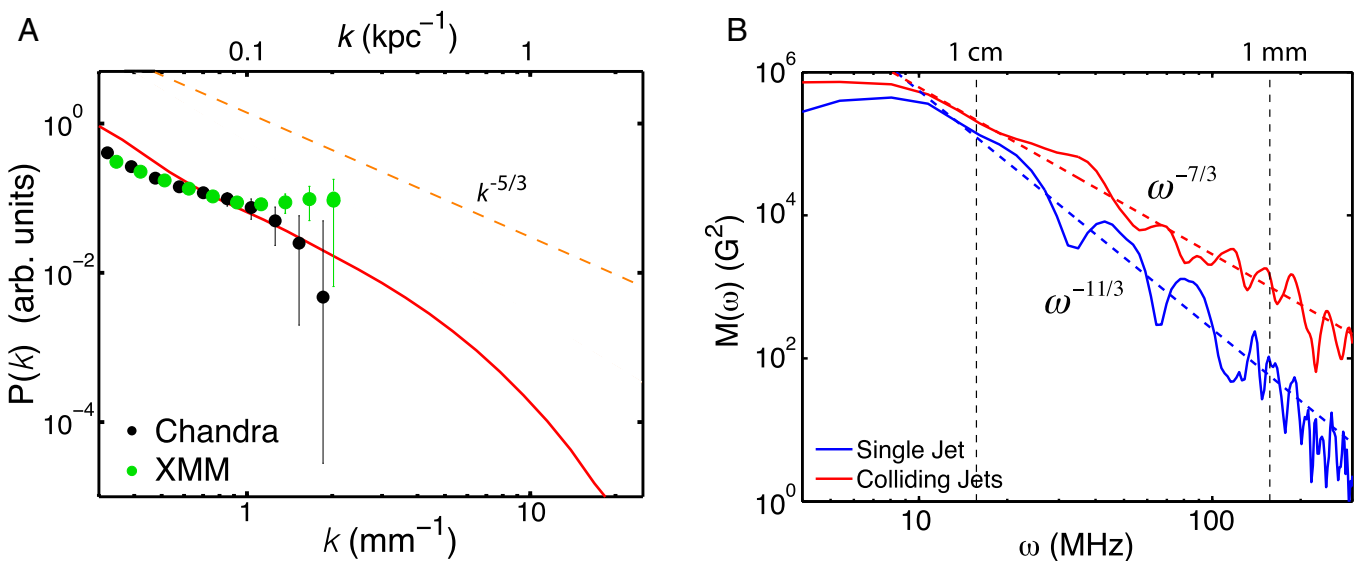


**Fig. 3.** Power spectra of turbulence. (A) Plot of the density fluctuation power spectrum  $P(k) = |n_k/n_0|^2$ , where  $n_k$  is the discrete Fourier transform of the space-dependent electron density and  $n_0$  is its average value. In Schlieren imaging, the measured signal intensity is proportional to  $\int (\partial n/\partial y + \partial n/\partial z) dx$ , where  $n$  is the electron density,  $x, y$  are the image plane spatial coordinates, and  $z$  is the depth (35). Therefore, under the assumption that turbulence is statistically homogeneous across the jet interaction region, the discrete Fourier transform of the central region of the jet collision in Fig. 1C directly gives  $n_k$ . The power spectrum is arbitrarily normalized so that  $P(k) \approx 1$  at the largest scale. The solid red curve corresponds to the experimental data, while the black and green symbols correspond to the inferred density spectrum in the Coma cluster obtained from CHANDRA and XMM satellite observations, respectively (25). (B) Plot of the magnetic energy spectrum  $M(\omega) = |B(\omega)|^2$ , where  $B(\omega)$  is the discrete Fourier transform of the total magnetic field for the cases both with a single jet (blue solid line) and with colliding jets (red solid line). The slope of the spectrum in the case of colliding jets is shallower than in the case of a single jet (where it is consistent with the  $k^{-11/3}$  Golitsyn spectrum, assuming conversion from frequencies to wavenumbers according to Taylor hypothesis,  $\omega \approx v_0 k$ ). This gradual shallowing of the spectrum with increasing Rm is a signature of the dynamo precursor regime (31). The measured frequency spectrum,  $\sim \omega^{-7/3}$ , can be argued to correspond to wavenumber spectrum,  $\sim k^{-1.9}$ , in the case of colliding jets, where Taylor’s hypothesis is inapplicable (see [Supporting Information](#)).



1. Miniati F, et al. (2000) Properties of cosmic shock waves in large-scale structure formation. *Astrophys J* 542:608–621.
2. Norman ML, Bryan GL (1999) *Cluster Turbulence*, Lecture Notes in Physics, eds Röser HJ, Meisenheimer K (Springer, Berlin), Vol 530.
3. Miniati F (2014) The Matryoshka run: A Eulerian refinement strategy to study the statistics of turbulence in virialized cosmic structures. *Astrophys J* 782(1):21.
4. Govoni F, Ferretti L (2004) Magnetic fields in clusters of galaxies. *Int J Mod Phys D* 13: 1549–1594.
5. Bernet ML, Miniati F, Lilly SJ, Kronberg PP, Dessauges-Zavadsky M (2008) Strong magnetic fields in normal galaxies at high redshift. *Nature* 454(7202):302–304.
6. Parker EN (1955) Hydromagnetic dynamo models. *Astrophys J* 122:293–314.
7. Zweibel EG, Heiles C (1997) Magnetic fields in galaxies and beyond. *Nature* 385: 131–136.
8. Schekochihin AA, Cowley SC (2006) Turbulence, magnetic fields, and plasma physics in clusters of galaxies. *Phys Plasmas* 13:056501.
9. Ryu D, Kang H, Cho J, Das S (2008) Turbulence and magnetic fields in the large-scale structure of the universe. *Science* 320(5878):909–912.
10. Meinecke J, et al. (2014) Turbulent amplification of magnetic fields in laboratory laser-produced shock waves. *Nat Phys* 10:520–524.
11. Schlickeiser R, Shukla PK (2003) Cosmological magnetic field generation by the Weibel instability. *Astrophys J* 599:L57–L60.
12. Medvedev MV, Silva LO, Kamionkowski M (2006) Cluster magnetic fields from large-scale Structure and galaxy cluster shocks. *Astrophys J* 642:L1–L4.
13. Huntington CM, et al. (2015) Observation of magnetic field generation via the Weibel instability in interpenetrating plasma flows. *Nat Phys* 11:173–176.
14. Park HS, et al. (2015) Collisionless shock experiments with lasers and observation of Weibel instabilities. *Phys Plasmas* 22(5):056311.
15. Langer M, Aghanim N, Puget J (2005) Magnetic fields from reionisation. *Astron Astrophys* 443:367–372.
16. Miniati F, Bell AR (2011) Resistive magnetic fields at cosmic dawn. *Astrophys J* 729:73.
17. Harrison ER (1970) Generation of magnetic fields in the radiation era. *Mon Not R Astron Soc* 147:279–286.
18. Durrer R, Neronov A (2013) Cosmological magnetic fields: Their generation, evolution and observation. *Astron Astrophys Rev* 21:62.
19. Ryutov D, et al. (1999) Similarity criteria for the laboratory simulation of supernova hydrodynamics. *Astrophys J* 518:821–832.
20. Cross JE, Reville B, Gregori G (2014) Scaling of magneto-quantum-radiative hydrodynamic equations: From laser-produced plasmas to astrophysics. *Astrophys J* 795:59.
21. Tzeferacos P, et al. (2012) Magnetohydrodynamic simulations of shock-generated magnetic field experiments. *High Energy Density Phys* 8:322–328.
22. Tzeferacos P, et al. (2014) FLASH MHD simulations of experiments that study shock-generated magnetic fields. *High Energy Density Phys*, 10.1016/j.hedp.2014.11.003.
23. Zhuravleva I, et al. (2014) Turbulent heating in the X-ray brightest galaxy clusters. *Nature* 515(7525):85–87.
24. Schuecker P, Finoguenov A, Miniati F, Böhringer H, Briel U (2004) Probing turbulence in the Coma galaxy cluster. *Astron Astrophys* 426:387–397.
25. Churazov E, et al. (2012) X-ray surface brightness and gas density fluctuations in the Coma cluster. *Mon Not R Astron Soc* 421:1123–1135.
26. Zhuravleva I, et al. (2014) The relation between gas density and velocity power spectra in galaxy clusters: Qualitative treatment and cosmological simulations. *Astrophys J* 788:L13.
27. Larson RB (1981) Turbulence and star formation in molecular clouds. *Mon Not R Astron Soc* 194:809–826.
28. Federrath C (2013) On the universality of supersonic turbulence. *Mon Not R Astron Soc* 436:1245–1257.
29. Golitsyn GS (1960) Fluctuations of the magnetic field and current density in a turbulent flow of a weakly conducting fluid. *Sov Phys Dokl* 5:536–539.
30. Moffatt HK (1961) The amplification of a weak applied magnetic field by turbulence in fluids of moderate conductivity. *J Fluid Mech* 11:625–635.
31. Schekochihin AA, et al. (2007) Fluctuation dynamo and turbulent induction at low magnetic Prandtl numbers. *New J Phys* 9:300.
32. Biermann L (1950) Über den Ursprung der Magnetfelder auf Sternen und im interstellaren Raum. *Z Naturforsch A* 5:65–71.
33. Gregori G, et al. (2012) Generation of scaled protogalactic seed magnetic fields in laser-produced shock waves. *Nature* 481(7382):480–483.
34. MacFarlane J, Golovkin I, Wang P, Woodruff P, Pereyra N (2007) Spect3d—A multi-dimensional collisional-radiative code for generating diagnostic signatures based on hydrodynamics and PIC simulation output. *High Energy Density Phys* 3:181–190.
35. Settles GS (2001) *Schlieren and Shadowgraph Techniques* (Springer, Berlin).
36. Fryxell B, et al. (2000) FLASH: An adaptive mesh hydrodynamics code for modeling astrophysical thermonuclear flashes. *Astrophys J* 131:S273–S334.
37. Dubey A, et al. (2009) Extensible component-based architecture for FLASH, a massively parallel, multiphysics simulation code. *Parallel Comput* 35(10-11):512–522.
38. Lee D (2013) A solution accurate, efficient and stable unsplit staggered mesh scheme for three dimensional magnetohydrodynamics. *J Comput Phys* 243:269–292.
39. Fatenejad M, et al. (2013) Modeling HEDLA magnetic field generation experiments on laser facilities. *High Energy Density Phys* 9:172–177.
40. Li S (2005) An HLLC Riemann solver for magneto-hydrodynamics. *J Comput Phys* 203: 344–357.
41. Kerley S (1972) Equation of state and phase diagram of dense hydrogen. *Phys Earth Planet Inter* 6:78–82.
42. Zel'dovich YB, Raizer YP (1966) *Physics of Shock Waves and High Temperature Hydrodynamic Phenomena* (Academic, New York).
43. MacFarlane J, Golovkin I, Woodruff P (2006) HELIOS-CR—A 1-D radiation-magneto-hydrodynamics code with inline atomic kinetics modeling. *J Quant Spectrosc Radiat Transfer* 99:381–397.
44. McWhirter RWP (1978) Review paper A5. Data needs, priorities and accuracies for plasma spectroscopy. *Phys Rep* 37(2):165–209.
45. Tsakiris GD, Eidmann K (1987) An approximate method for calculating Planck and Rosseland mean opacities in hot, dense plasmas. *J Quant Spectrosc Radiat Transfer* 8: 353–368.
46. Malagoli A, Rosner R, Bodo G (1987) On the thermal instability of galactic and cluster halos. *Astrophys J* 319:632–636.
47. Taylor GI (1938) The spectrum of turbulence. *Proc R Soc Lond A Math Phys Sci* 164: 467–490.
48. Park H-S, et al. (2012) Studying astrophysical collisionless shocks with counter-streaming plasmas from high power lasers. *High Energy Density Phys* 8:38–45.
49. Drake RP, Gregori G (2012) Design considerations for unmagnetized collisionless-shock measurements in homologous flows. *Astrophys J* 479:171.
50. Kato TN, Takabe H (2008) Nonrelativistic collisionless shocks in unmagnetized electron-ion plasmas. *Astrophys J* 681:L93–L96.
51. Ichimaru S (2004) *Statistical Plasma Physics* (Westview, Boulder, CO).